Wavelength locking to CO_2 absorption line-center for 2-μm pulsed IPDA lidar application

Tamer F. Refaat*, Mulugeta Petros, Charles W. Antill, Upendra N. Singh and Jirong Yu
NASA Langley Research Center, 5 N Dryden Street, MS 468, Hampton, VA, USA 23681

ABSTRACT

An airborne 2-μm triple-pulse integrated path differential absorption (IPDA) lidar is currently under development at NASA Langley Research Center (LaRC). This IPDA lidar system targets both atmospheric carbon dioxide (CO_2) and water vapor (H_2O) column measurements. Independent wavelength control of each of the transmitted laser pulses is a key feature for the success of this instrument. The wavelength control unit provides switching, tuning and locking for each pulse in reference to a 2-μm CW laser source locked to CO_2 line-center. Targeting the CO_2 R30 line center, at 2050.967 nm, a wavelength locking unit has been integrated using semiconductor laser diode. The CO_2 center-line locking unit includes a laser diode current driver, temperature controller, center-line locking controller and CO_2 absorption cell. This paper presents the CO_2 center-line locking unit architecture, characterization procedure and results. Assessment of wavelength jitter on the IPDA measurement error will also be addressed by comparison to the system design.

Keywords: Active remote sensing, carbon dioxide, IPDA lidar, triple-pulse laser, wavelength locking, mid IR laser

1. INTRODUCTION

NASA Langley Research Center (LaRC) is currently developing a state-of-the-art triple-pulse integrated path differential absorption (IPDA) lidar instrument [1]. This instrument is an update of the previously demonstrated 2-μm double-pulse IPDA lidar for atmospheric carbon dioxide (CO_2) measurement [2-3]. The objective of the triple-pulse instrument is to enhance the active remote sensing capabilities of the previous instrument by including atmospheric water vapor (H_2O) measurement [3]. The triple pulse IPDA lidar transmitter generates three successive pulses separated by 200 μsec at a repetition rate of 50 Hz. These three pulses are independently tuned to three different wavelengths. The final product would be an IPDA instrument that measures both CO_2 and H_2O differential optical depths simultaneously and independently [4]. IPDA differential optical depth measurement can be converted into a weighted average column dry-air volume-mixing ratio through weighting functions. Weighting functions depends on meteorology and spectroscopy, which do not vary on a shot-to-shot basis. Therefore, the retrieval of the weighted average column dry-air volume-mixing ratio of the gases is dominated by the accuracy of the IPDA lidar optical depth measurements. Errors in CO_2 and H_2O differential optical depth measurements through the IPDA technique result from random and systematic sources. Random errors associated with the IPDA signals are dominated by the detection system and it can be significantly reduced by shot averaging. IPDA lidar systematic errors are associated with the precise knowledge of the atmospheric environment (atmospheric errors) and laser transmitter performance (transmitter errors) [4].

Significant transmitter systematic errors result from the spectral quality of the laser beam and locking control of the selected operational wavelengths. Transmitted laser spectral quality translates to line-width errors, while locking control translates to wavelength jitter. Depending on the instrument setting and measurement conditions, transmitter errors could dominate the total IPDA error budget. A previous study showed that on-line wavelength jitter is the dominant error source among different transmitter systematic errors for both CO_2 and H_2O measurements. As an example, on-line laser wavelength jitter errors of 0.04% and 0.05% for CO_2 and H_2O, respectively, would dominated the gases surface measurements as compared to less than 0.001% from other transmitter errors [4]. The study assumes triple pulse IPDA airborne nadir operation from 8 km altitude and ±1 MHz wavelength jitter. The significance of the IPDA sensing wavelength jitter drives the need for a precise wavelength locking mechanism to reduce such error. This is achieved through the design of a wavelength control unit that provides switching, tuning and locking for the wavelength of each pulse relative to the CO_2 R30 absorption line center wavelength, λ_C, of 2050.967 nm. The objective is to seed these pulses with 2051.059 nm, 2051.1915 nm and 2050.5094 nm wavelengths, equivalent to 6, 16 and 32 GHz shifts form λ_C [4]. Wavelength generation of seed pulses is referenced to a 2-μm CW laser source locked to λ_C.

*tamer.f.refaat@nasa.gov; phone 1 757 864-1540; fax 1 757 864-8828

Different 2-μm CW laser source technologies were investigated for this application. These include a solid-state laser (Coherent Technology Inc.), a fiber laser (AdValue Photonics) and a semiconductor laser (NASA JPL). The suitability of the laser source for this application was compared through different performance parameters, including output power, single frequency operation, short and long term wavelength stability, tuning range and speed, locking stability, power consumption, size and weight. Solid-state lasers have been previously applied and successfully demonstrated for center-line locking. Nevertheless, commercial unavailability and complexity were motivation to search for a new source. As a result, a semiconductor laser was selected for the current triple-pulse IPDA lidar center line locking application. This semiconductor laser is based on a GaSb single-mode distributed-feedback design that is newly developed at NASA Jet Propulsion Laboratory (JPL) [5-6]. The source was packaged inside a standard 14-pin butterfly package with an optical fiber pigtail output (Nufern-PM1950) and an integrated single-stage optical isolator to suppress optical feedback into the laser cavity. Packaging also includes a thermoelectric cooler and a thermistor for device temperature control. Reports indicate that the device shows single mode behavior with better than 50 dB of side-mode suppression ratio and exhibit stable and constant wavelength tuning of 0.18 nm/K over large current and temperature ranges [5]. In this paper, the application of this laser for wavelength locking to a CO_2 absorption line-center will be presented. This includes device characterization and wavelength tuning to a CO_2 reference gas cell. This will generate the reference wavelength for the triple pulse IPDA lidar instrument for atmospheric CO_2 and H_2O active remote sensing.

2. PRINCIPLE OF WAVELENGTH LOCKING

Wavelength locking relies on a CO_2 absorption gas cell, shown in figure 1. The cell is filled with pure CO_2 gas at the low pressure of 666.612 Pascal (5 Torr). A 2-μm source is applied to a side window and after several reflections, equivalent to 10 m absorption path length, L, the output beam is detected with a 2-μm InGaAs pin detector. The measured power of the output beam, P, depends on the source wavelength, λ, assuming constant input power, P_o, and according to the Beer-Lambert law given by

$$P(\lambda) = P_o \cdot \exp\left[-N \cdot \sigma(\lambda) \cdot L\right] \tag{1}$$

where σ is the absorption cross section and N is the number density of the CO_2 gas molecules inside the cell. The number density is obtained by applying the Ideal Gas law and assuming room temperature of 300 K results in a CO_2 number density of 1.61×10^{23} m^{-3}. Figure 2 shows the CO_2 absorption spectra under these conditions. The figure also shows the gas cell transmission, equivalent to the exponential term of equation (1). If the input 2-μm source is modulated to two different side-line wavelengths with an offset of $\Delta\lambda$, by an electro-optic (EO) modulator for example, and a heterodyne technique is applied to the detected signal, an error signal, ε, would result according to

$$\varepsilon = P(\lambda + \Delta\lambda) - P(\lambda - \Delta\lambda). \tag{2}$$

Figure 2 shows the error signal variation with wavelength. A precise center-line locking controller was designed to detect this error signal. The error signal is minimized by tuning the 2-μm source, which results in side-lines shift to equate their output power. This results in setting the source wavelength around the zero line crossing of the error signal equivalent to the peak absorption wavelength, assuming perfect CO_2 absorption line symmetry.

3. SEMICONDUCTOR LASER CHARACTERISTICS

Two 2-μm semiconductor laser diode (LD) devices were acquired from NASA JPL. The LD output power and wavelength are functions of the device drive current and operating temperature. Therefore, an LD current driver and temperature controllers were designed, fabricated and packaged at NASA LaRC. The LD current driver is capable of producing 0 to 400 mA, with 0.1 mA resolution. Two temperature controllers were used to control both the LD device temperature and the case of the butterfly package. This results in a LD temperature set range of 15 to 25ºC, with 0.1 mK resolution. Figure 3 shows the packaged LD with the current drive and temperature control unit as well as the center line locking unit. A graphical user interface (GUI) was programed to set the LD operating conditions and limits. In addition, the electronic design allows either internal or external LD current modulation and provides modulation monitor signal. In all experiments, the case temperature was set to a fixed value of 18ºC. An external fiber isolator was coupled to the LD fiber output to enhance optical feedback suppression. Figure 4 shows a Fabry-Perot (Burleigh: RG-91) scan for the LD output. The scan confirms single frequency operation of the device, which is a critical requirement for the CO_2 absorption line center locking.

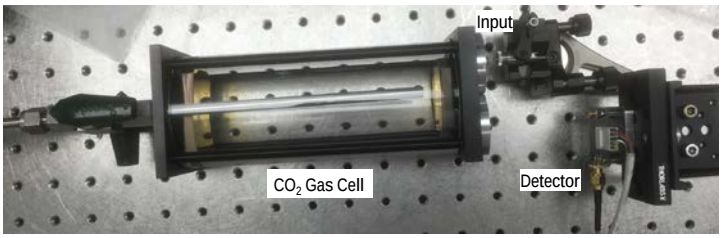

Figure 1. Pure CO_2 absorption gas cell with fiber collimator at the input to apply the 2-μm radiation source and a detector at the output that feeds to the center line locking controller.

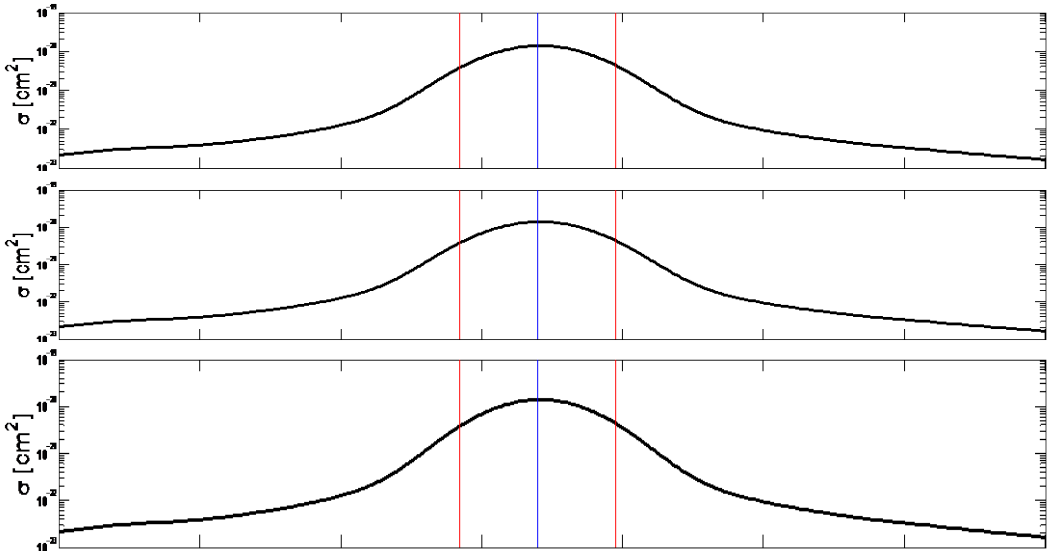

Figure 2. Simulation of the wavelength locking principle. The CO_2 absorption cross section (top) was calculated using the HITRAN data base for line parameters assuming Voigt line profile at the cell pressure of 666.612 Pascal and temperature of 300 K. Ideal Gas law was applied to estimate the gas number density and the cell transmission (middle). By modulating the source and error signal is generated (bottom). Vertical red lines mark the modulation side-lines and blue line mark the CO_2 absorption line center.

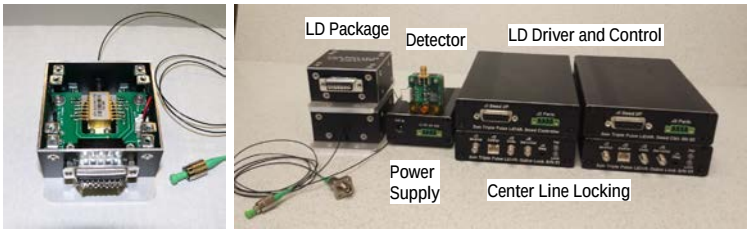

Figure 3. Packaged LD enclosure (left) and LD current driver and temperature controller units and center line locking units (right). Duplicate electronics were integrated for both devices, including power supplied and the CO_2 cell detector. LD and electronics enclosures sizes are 6.5×6×4 and 16.5×11×3 cm^3, respectively.

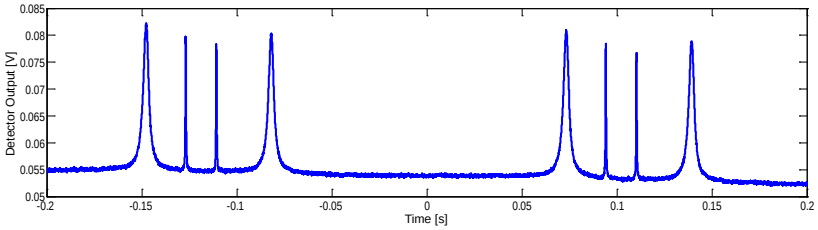

Figure 4. Fabry-Perot driver (top) and detector output scan (bottom) for the output of the LD. LD drive current is 183.6 mA and temperature is 23ºC. Scan confirms single frequency operation of the LD device.

The LD output power was measured using an optical power meter (Melles Griot: Broadband Power/Energy Meter 13PEM001) at different drive currents and set device temperatures, as shown in figure 5. Wavelength measurements were conducted, at the same temperature and current setting, using a wavelength meter (Bristol: 621), as shown in the same figure. LD current limits were set to a minimum of 50 mA, equal to the threshold current, and a maximum of 250 mA defined by the manufacturer, with 10 mA steps. A third-order polynomial fit was applied to the LD power output, P_o, and wavelength, λ, versus drive current, I, for each temperature setting, according to the equations

$$P_o = \sum_{n=0}^{3} a_n \cdot I^n \qquad \& \qquad \lambda = \sum_{n=0}^{3} b_n \cdot I^n \tag{3}$$

where a_n and b_n are the power and wavelength fitting parameters, respectively, as listed in Table 1 and n is the fitting order. Comparing the LD wavelength measurements to the CO_2 absorption line center wavelength indicated the suitability of the device as the radiation source of choice for this application. Current and temperature set values of 183.6 mA and 23ºC, respectively, were selected for the LD operation that would produce an output radiation with close wavelength to the target locking and sufficient power without electronic overload. For the selected LD operation settings, figure 6 shows the long term power and wavelength stabilities. Long term LD output power stability was conducted with more than 2.2 M samples collected through 83 minutes. Statistical analysis was conducted by observing the occurrences of each power level, as shown in figure 6. Then, the data was fitted to a Gaussian distribution that resulted in a measured power mean and standard deviation of 5.97±0.05 mW. This translates to 0.84% LD output power stability. The same procedures were applied to obtain the wavelength long term stability. About 12.5 k wavelength samples were collected during 77 minutes and the occurrences were observed for 0.01 pm wavelength bins. Gaussian fitting resulted in a mean and standard deviation of 2050.9665 nm and 0.086 pm, respectively. This standard deviation translates to ±6.1 MHz wavelength jitter, considering that 1 pm wavelength is equivalent to 71.2 MHz frequency shift at λ_C. This drives the need for more precise center line locking electronics.

The LD current was externally modulated using a low frequency sinusoidal signal with a low frequency of 20 mHz, as shown in figure 7a. The LD output was applied to the input of the CO_2 absorption cell. Monitoring the modulation current, and applying equations (3) result in the LD output wavelength and power, shown in figures 7b and 7c. The calibrated wavelength was compared to simultaneous measurement indicating 0.1 pm wavelength uncertainty. The cell output power, shown in figure 7d, confirms the gas absorption. Figure 8 focuses on the cell transmission calculation obtained as the ratio of the cell output to input powers of figure 7, after folding time profiles by wavelength conversion (i.e., converting the independent variable from time to wavelength). Transmission loss of about 50% and 4.4 pm (313.3 MHz) full-with-half-max (FWHM) are suitable for the center line locking electronics requirements.

4. CO_2 ABSORPTION LINE CENTER LOCKING

The setup for the CO_2 absorption line center locking is shown in figure 9. Center line locking (CLL) electronics drives a 200 MHz EO modulator to generate two wavelengths offsets ±2.78 pm from λ_C. The modulated output is collimated and applied to the gas cell. The cell output is detected and fed back to the CLL electronics to sense the error signal. CLL is capable of operating in a free-running mode or locked mode. In free-running mode the CLL does not control the LD driver, which is useful for diagnostics through the error and detector monitors. In locked-mode, the CLL will control the LD current driver, through the servo signal, to precisely lock the LD output wavelength. The free-running mode was used to investigate the influence of the cell pressure on the detector and error signals. Figure 10 shows the variation of these signals at different pressure. The objective is to compare the zero crossing with the locking wavelength, while maximizing the error peak-to-peak value, as indicated in the figure. This results in an optimum cell pressure of 7.3 Torr. Figure 11 shows the monitor signals at this pressure setting in the free-running mode. The LD current driver internal modulation is a triangle wave that results in a wavelength scan according to equation (3). The detector and error monitors were folded and averaged as a function of wavelength as presented in the previous section. Using the CLL locked mode results in a precise wavelength locking as shown in figure 12. The figure compares the error signal for the CLL free-running and locked modes. The figure also presents the statistical analysis and fitting for 1 M samples and indicates wavelength mean and standard deviation of 2050.966967 nm and 0.00913 pm, respectively. This standard deviation translates to ±650.1 kHz wavelength jitter. This indicates the success of the CO_2 absorption line center locking source, electronics and methodology for the triple-pulse IPDA lidar application.

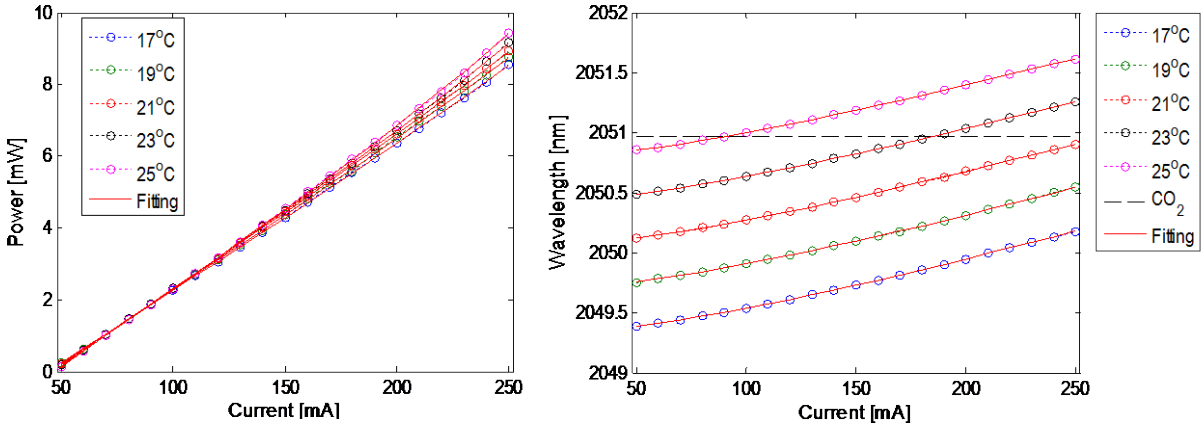

Figure 5. Measurements and curve fittings of the 2-μm LD output power (left) and wavelength (right) variations with drive current at different temperature settings. Horizontal dashed line marks the CO_2 absorption line center locking target.

Table 1. Polynomial fitting parameters for laser diode output power and wavelength versus drive current at different temperatures.

a_0	a_1	a_2	a_3	b_0	b_1	b_2	b_3	T [°C]
-1.796	4.127E-2	-1.144E-5	4.513E-8	2049.281	1.490E-3	1.235E-5	-1.557E-8	17
-1.822	4.124E-2	-5.825E-6	3.933E-8	2049.648	1.614E-3	1.110E-5	-1.267E-8	19
-1.950	4.353E-2	-1.529E-5	5.968E-8	2050.023	1.373E-3	1.306E-5	-1.775E-8	21
-2.073	4.614E-2	-3.334E-5	1.123E-7	2050.387	1.432E-3	1.245E-5	-1.662E-8	23
-2.114	4.603E-2	-3.019E-5	1.208E-7	2050.779	0.765E-3	1.727E-5	-2.765E-8	25

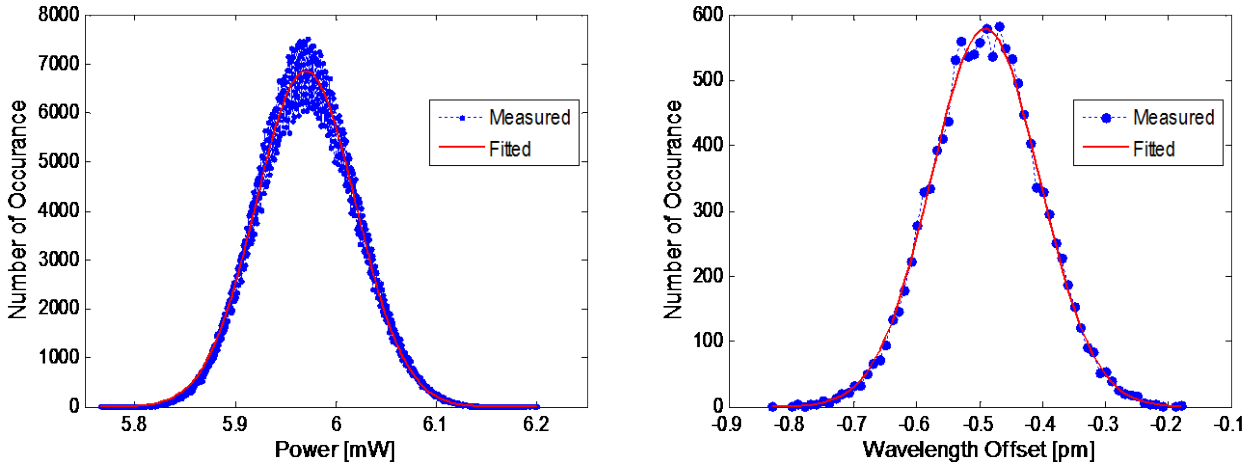

Figure 6. Statistical analysis and Gaussian fitting of the un-locked long term stability records for the 2-μm LD power (left) and wavelength (right). Results indicated output power mean of 5.97 mW and standard deviation of 0.05 mW. Wavelength results indicated 2050.9665 nm mean and 0.086 pm standard deviation. This standard deviation translates to ±6.1 MHz wavelength jitter.

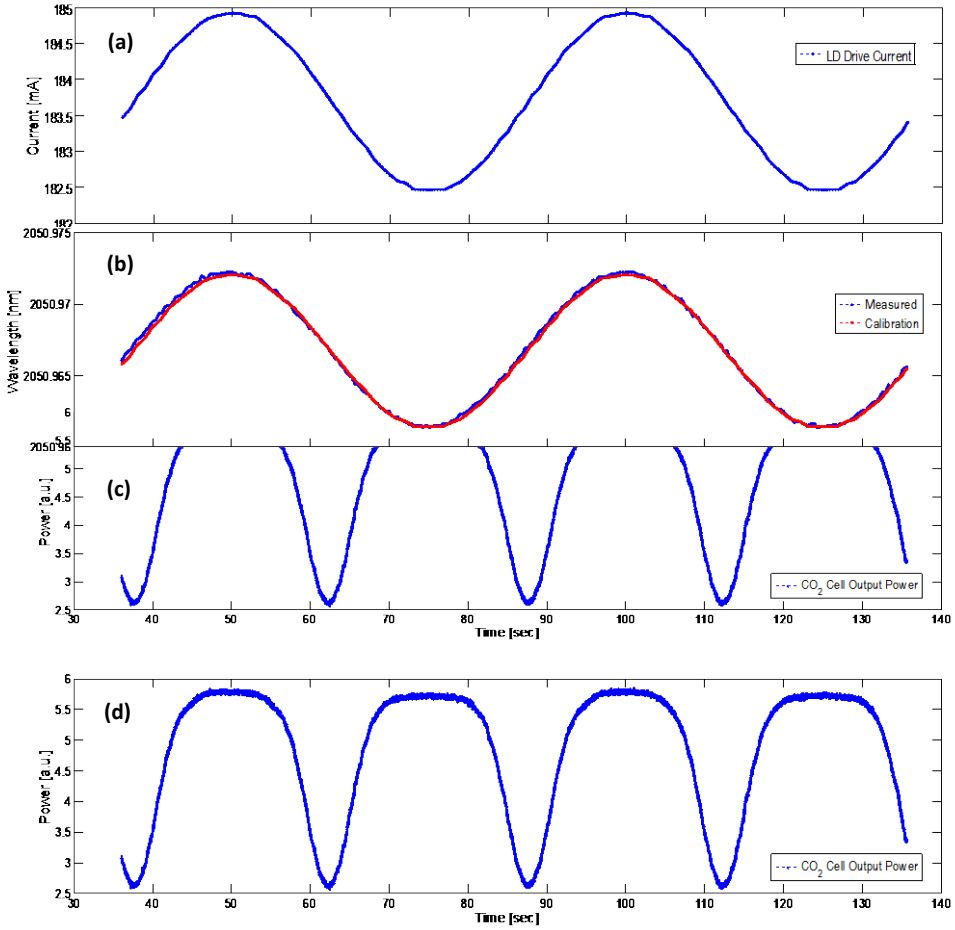

Figure 7. External sinusoidal modulation of the LD current (a) and the resulted wavelength (b) and the corresponding output power (c) applied to the CO_2 absorption cell input and the cell output power (d).

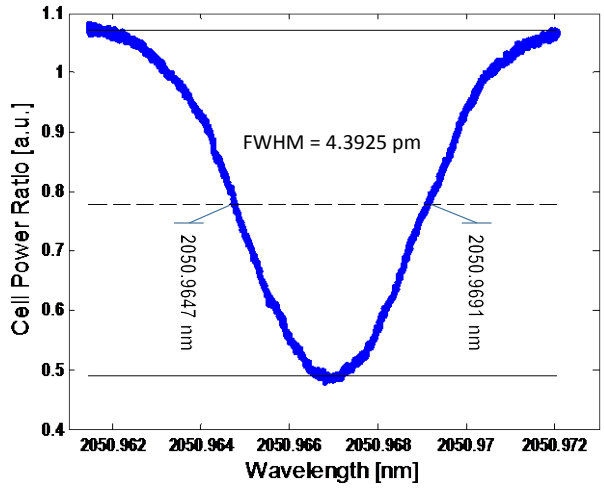

Figure 8. CO_2 cell transmission calculation obtained as the ratio of the cell output power, of figure 7d, to the cell input power, of figure 7c. Independent variable was converted from time to wavelength, of figire 7b.

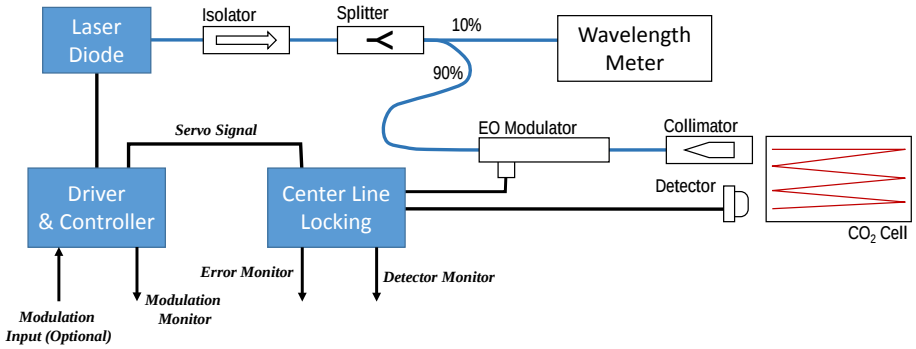

Figure 9. Experimental setup of the CO_2 absorption line center locking. CCL electronics drives a 200 MHz EO modulator to generate two wavelengths offsets. Modulated output is collimated and applied to the CO_2 cell, the output of which is detected and feedback to CLL electronics. CLL is capable of operating in a free-running mode or locked mode through the servo enable signal.

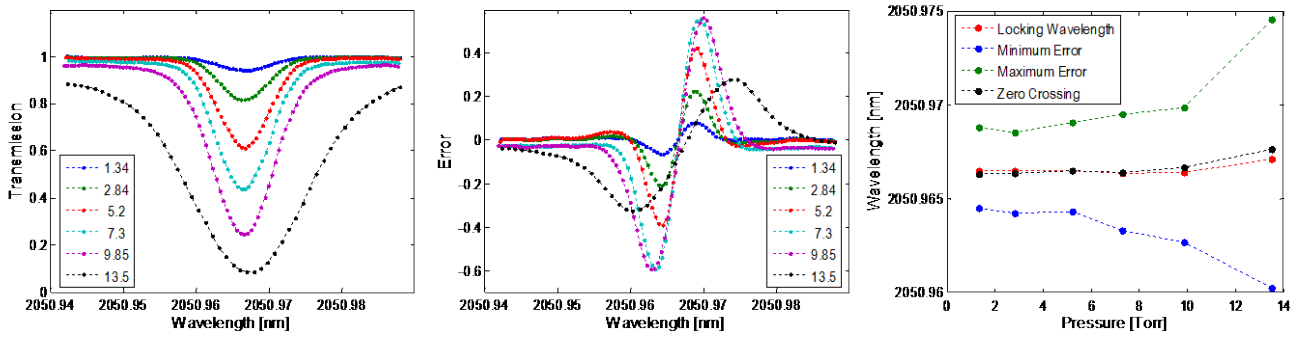

Figure 10. Detector monitor (left) and error monitor (middle) signals variation with the CO_2 cell pressure. Comparison of zero crossing wavelength with locking wavelength and the error peak values (right).

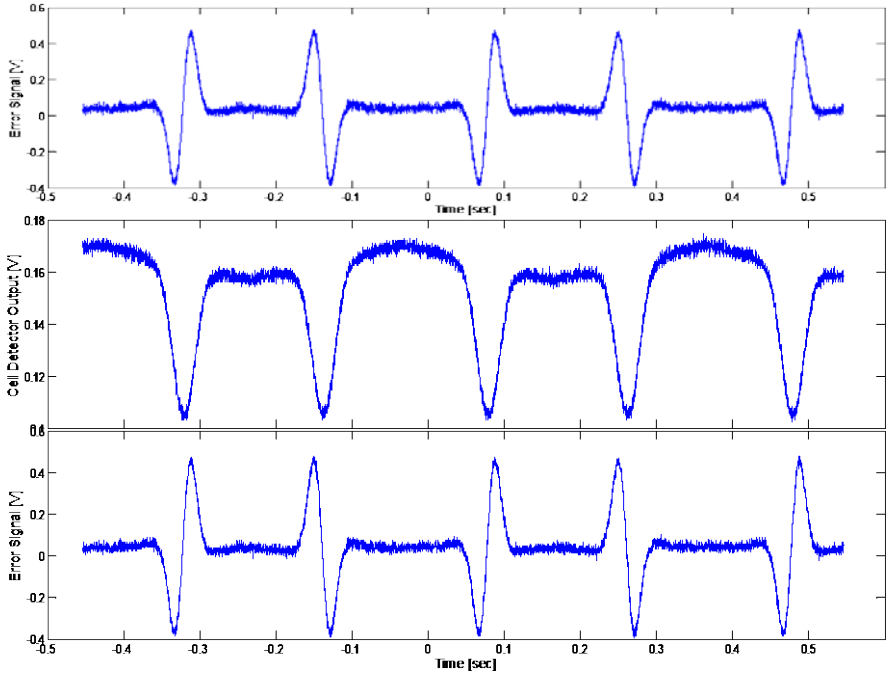

Figure 11. Internal LD current modulation monitor (top), cell detector monitor (middle) and error signal monitor (bottom) for 7.3 Torr CO_2 pressure with CLL in free-running mode.

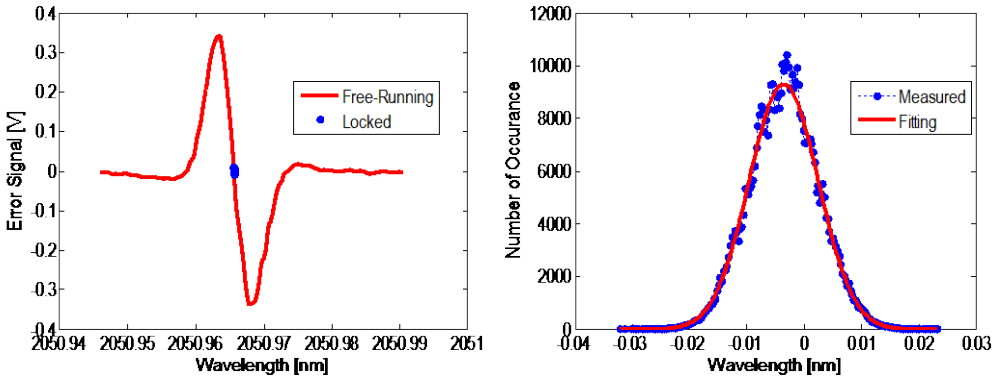

Figure 12. Comparison of the error signals for the CLL free-running and locked modes (left). Statistical analysis and Gaussian fitting (right) of the locked wavelength. Results indicated wavelength mean and standard deviation of 2050.966967 nm and 0.00913 pm, respectively. This standard deviation translates to ±650.1 kHz wavelength jitter.

5. CONCLUSION

NASA LaRC is developing a triple-pulse IPDA lidar instrument for simultaneous and independent CO_2 and H_2O measurements. This instrument is an upgrade of the previously demonstrated 2-μm CO_2 double-pulse IPDA lidar. A study indicated that ±1 MHz on-line wavelength jitter is the dominant transmitter systematic error source for this instrument. This drives the need for a precise wavelength locking mechanism to reduce such error. The design and results for a CO_2 absorption line center locking technique was presented. The design is based on a tunable CW 2-μm semiconductor laser diode developed at NASA JPL. Driver electronics, controllers and center line locking electronics were developed at NASA LaRC. Diode testing and characterization were conducted at NASA LaRC resulting in a wavelength jitter of ±6.1 MHz. This jitter is significantly enhanced to ±650.1 kHz using the center line locking electronics. This meets the objective of jitter limit of less than ±1MHz. This indicates the success of the laser source for this application. IPDA modeling will be updated to accommodate the new findings.

ACKNOWLEDGEMENT

The authors acknowledge the continual support from NASA Earth Science technology Office

REFERENCES

[1] U. Singh, T. Refaat, M. Petros and J. Yu, “triple-pulsed two-micron integrated path differential absorption lidar: a new active remote sensing capability with path to space,” in Proceedings of the 27th International Laser Radar Conference, New York, NY, 2015.

[2] U. Singh, J. Yu, M. Petros, T. Refaat, R. Remus and K. Reithmaier, “Development of double- and triple-pulsed 2-micron IPDA lidars for column CO_2 measurements”, Proc. of SPIE 9612, 961204, 2015.

[3] U. Singh, T. Refaat, J. Yu, M. Petros and R. Remus, “Airborne active remote sensor for atmospheric carbon dioxide”, SPIE Newsroom, 2015.

[4] T. Refaat, U. Singh, J. Yu, M. Petros, S. Ismail, M. Kavaya, and K. Davis, “Evaluation of an airborne triple-pulsed 2-μm IPDA lidar for simultaneous and independent atmospheric water vapor and carbon dioxide measurements”, Applied Optics 54, 1387-1398, 2015.

[5] M. Bagheri, G. Spiers, C. Frez, S. Forouhar, and F. Aflatouni, “Linewidth measurement of distributed-feedback semiconductor lasers operating near 2.05 μm”, IEEE Photonics Technology Letters 27, 1934-1937, 2015.

[6] S. Forouhar, R. Briggs, C. Frez, K. Franz, and A. Ksendzov, “High power laterally coupled distributed-feedback GaSb-based diode lasers at 2 μm wavelength,” Applied Physics Letters 100, 031107, 2012.